

FAR-INFRARED PROPERTIES OF INFRARED BRIGHT DUST-OBSCURED GALAXIES SELECTED WITH IRAS AND AKARI FAR-INFRARED ALL-SKY SURVEY

YOSHIKI TOBA¹, TOHRU NAGAO², WEI-HAO WANG¹, HIDEO MATSUHARA^{3,4}, MASAYUKI AKIYAMA⁵, TOMOTSUGU GOTO⁶, YUSEI KOYAMA^{7,8}, YOUICHI OHYAMA¹, ISSEI YAMAMURA^{3,4}

¹Academia Sinica Institute of Astronomy and Astrophysics, PO Box 23-141, Taipei 10617, Taiwan

²Research Center for Space and Cosmic Evolution, Ehime University, Bunkyo-cho, Matsuyama, Ehime 790-8577, Japan

³Institute of Space and Astronautical Science, Japan Aerospace Exploration Agency, 3-1-1 Yoshinodai, Chuo-ku, Sagami-hara, Kanagawa 252-5210, Japan

⁴Department of Space and Astronautical Science, SOKENDAI (The Graduate University for Advanced Studies), 3-1-1 Yoshinodai, Chuo-ku, Sagami-hara, Kanagawa 252-5210, Japan

⁵Astronomical Institute, Tohoku University, Aramaki, Aoba-ku, Sendai 980-8578, Japan

⁶Institute of Astronomy and Department of Physics, National Tsing Hua University, No. 101, Section 2, Kuang-Fu Road, Hsinchu 30013, Taiwan

⁷Subaru Telescope, National Astronomical Observatory of Japan, National Institutes of Natural Sciences, 650 North A'ohoku Place, Hilo, HI 96720, U.S.A.

⁸Graduate University for Advanced Studies (SOKENDAI), Osawa 2-21-1, Mitaka, Tokyo 181-8588, Japan

ABSTRACT

We investigate the star forming activity of a sample of infrared (IR)-bright dust-obscured galaxies (DOGs) that show an extreme red color in the optical and IR regime, $(i - [22])_{\text{AB}} > 7.0$. Combining an IR-bright DOG sample with the flux at $22 \mu\text{m} > 3.8 \text{ mJy}$ discovered by Toba & Nagao (2016) with *IRAS* faint source catalog version 2 and *AKARI* far-IR (FIR) all-sky survey bright source catalog version 2, we selected 109 DOGs with FIR data. For a subsample of 7 IR-bright DOGs with spectroscopic redshift ($0.07 < z < 1.0$) that was obtained from literature, we estimated their IR luminosity, star formation rate (SFR), and stellar mass based on the spectral energy distribution fitting. We found that (i) *WISE* $22 \mu\text{m}$ luminosity at observed frame is a good indicator of IR luminosity for IR-bright DOGs and (ii) the contribution of active galactic nucleus (AGN) to IR luminosity increases with IR luminosity. By comparing the stellar mass and SFR relation for our DOG sample and literature, we found that most of IR-bright DOGs lie significantly above the main sequence of star-forming galaxies at similar redshift, indicating that the majority of *IRAS*- and/or *AKARI*-detected IR-bright DOGs are starburst galaxies.

Keywords: catalogs — galaxies: active — galaxies: star formation — infrared: galaxies

1. INTRODUCTION

The stellar mass (M_*) and the star formation rate (SFR) are two of the most fundamental and important physical quantities of galaxies. Since a tight correlation between M_* and SFR of galaxies has been discovered (e.g., Brinchmann et al. 2004), many authors have intensively investigated this relation for various galaxies at various redshift (e.g., Daddi et al. 2007; Elbaz et al. 2007; Noeske et al. 2007). It is well known that the majority of galaxies follows a relation

so-called “main sequence (MS)” and this correlation is seen to evolve towards high redshift across all environments (e.g., Whitaker et al. 2012; Koyama et al. 2013; Lee et al. 2015; Tomczak et al. 2016). However, a comprehensive implication of the tight correlation between stellar mass and SFR and of its redshift evolution is still unclear (see Casey et al. 2014). In addition, it is known that galaxies undergoing active star formation (SF) that could be induced by major merger process lie significantly above the MS and referred as starburst galaxies. Investigating the relation of these starburst galaxies and MS is important to understand the origin of the M_* -SFR connection.

In this work, we focus on dust-obscured galaxies (DOGs: [Dey et al. 2008](#)). Their mid-infrared (MIR) flux densities are three orders of magnitude larger than those at optical wavelengths, implying that a significant active galactic nucleus (AGN) and/or SF activities heat dust. The optical and ultraviolet (UV) emission originated from these activities is absorbed by heavily surrounding dust that re-emits in the IR wavelength. Their IR luminosity often exceeds $10^{12} L_{\odot}$ that is classified as ultraluminous IR galaxies (ULIRGs: [Sanders & Mirabel 1996](#)). Recently, [Riguccini et al. \(2015\)](#) investigated the far-IR (FIR) properties for a sample of 95 DOGs within the COSMOS field, based on spectral energy distribution (SED) fitting. However, their DOG sample is limited to those with flux density at $24 \mu\text{m}$ less than 3.0 mJy (its mean value is ~ 0.4 mJy). On the other hand, IR-bright DOGs with a much higher MIR flux density are thought to be a maximum phase of SF and AGN activity (e.g., [Hopkins et al. 2008](#)), and thus they are likely to be a crucial population to understand what kinds of physical processes drive the SFR– M_* relation. Recently, we successfully discovered a large number of IR-bright DOGs and investigated their statistical properties ([Toba et al. 2015](#); [Toba & Nagao 2016](#); [Toba et al. 2017](#)). However, their SF properties are still unknown because we lack deep and wide FIR data that are responsible for the SF activity.

In order to estimate the FIR luminosity of IR-bright DOGs and investigate their SF properties, we utilized data from the *Infrared Astronomical Satellite* (*IRAS*) and *AKARI* satellite. *IRAS* is the first satellite that performed an all-sky survey in four IR bands centered at 12, 25, 60, and 100 μm ([Neugebauer et al. 1984](#); [Beichman et al. 1988](#)). In this work, we utilized the *IRAS* Faint Source Catalogue (FSC), version 2.0 ([Moshir et al. 1992](#)) reaching a depth of ~ 0.2 Jy at 12, 25 and 60 μm and ~ 1.0 Jy at 100 μm . *AKARI* is the first Japanese space satellite dedicated to IR astronomy, that was launched in 2006 ([Murakami et al. 2007](#)). *AKARI* performed an all-sky survey at 9, 18, 65, 90, 140, and 160 μm whose spatial resolution and sensitivity are much higher than those of the *IRAS*. In this work, we utilized the *AKARI* Far-Infrared Surveyor (FIS: [Kawada et al. 2007](#)) bright source catalogue (BSC) version 2.0 (Yamamura et al. in prep.), which provides the positions and flux densities in the four FIR wavelengths centered at 65, 90, 140, and 160 μm . The 5σ sensitivity at each band is about 2.4, 0.55, 1.4, and 6.3 Jy, which is the deepest data in terms of the FIR all-sky data, and thus these data should be useful to derive the total IR luminosity and SFR of IR-bright DOGs.

In this paper, we present the IR luminosity, stellar mass, and SFR for IR-bright DOGs detected by the Sloan Digital Sky Survey (SDSS: [York et al.](#)

[2000](#)), *Wide-field Infrared Survey Explorer* (*WISE*: [Wright et al. 2010](#)), and at least detected by *IRAS* or *AKARI* FIR all-sky survey. These multi-wavelength data are critical for investigating where IR-bright DOGs lie in the SFR–stellar mass (SFR– M_*) plane. Throughout this paper, we adopt $H_0 = 70 \text{ km s}^{-1} \text{ Mpc}^{-1}$, $\Omega_M = 0.3$, and $\Omega_{\Lambda} = 0.7$. Unless otherwise noted, all magnitudes refer on the AB system.

2. DATA AND ANALYSIS

2.1. Sample selection

We selected 8 IR-bright DOGs with spectroscopic information based on *WISE*, SDSS, *IRAS*, and *AKARI* catalogs ¹. The flow chart of our sample selection process is shown in Figure 1.

The DOG parent sample (hereafter WISE–SDSS photo DOGs) was selected from [Toba & Nagao \(2016\)](#) who discovered 5,311 IR-bright DOGs with $i - [22] > 7.0$ and flux at 22 $\mu\text{m} > 3.8$ mJy, where i and $[22]$ are i -band and 22 μm AB magnitudes, respectively, based on the ALLWISE ([Cutri et al. 2014](#)) and SDSS Data Release 12 (SDSS DR12: [Alam et al. 2015](#)) catalogs. For them, we first cross-identified *IRAS* FSC version 2 that includes 173,044 sources. Before cross-matching, we conservatively selected 52,139 sources that are not affected by cirrus and confusion by adopting $\text{CIRRUS} = 0$ and $\text{CONFUSE} = 0$. Using a matching radius of $1'$, 59 DOGs (hereafter WISE–SDSS–*IRAS* DOGs) were selected. Note that we checked the quality of *IRAS* flux in each band (`fqual_12/25/60/100`) for them, and confirmed that flux at least in one band is measured with good quality (i.e., `fqual_12/25/60/100` ≥ 2). For $5,311 - 59 = 5,252$ DOGs that are not cross-identified with *IRAS* FSC (hereafter WISE–SDSS–non *IRAS* DOGs), we cross-identified *AKARI* FIR BSC version 2 that includes 918,054 sources. Before cross-matching, we limited ourselves to 501,444 sources with high detection reliability ($\text{GRADE} = 3$), i.e., detected by at least two wavelength bands or in four or more scans in one wavelength band. Using a matching radius of $20''$ which is determined by considering the point spread function size of $\sim 40''$ of the *AKARI* 90 μm data, 50 DOGs (hereafter WISE–SDSS–non *IRAS*–*AKARI* DOGs) were selected. Only one *AKARI* object has 2 counterpart candidates of WISE–SDSS photo DOGs within the search radius. We choose the nearest one as a counterpart. Note that we also cross-identified with *AKARI* FSC BSC ver.2. even for WISE–SDSS–*IRAS* DOGs to collect more FIR information for the matched sources. Consequently, we

¹ For the selection process, we employed the TOPCAT, which is an interactive graphical viewer and editor for tabular data ([Taylor et al. 2005](#)).

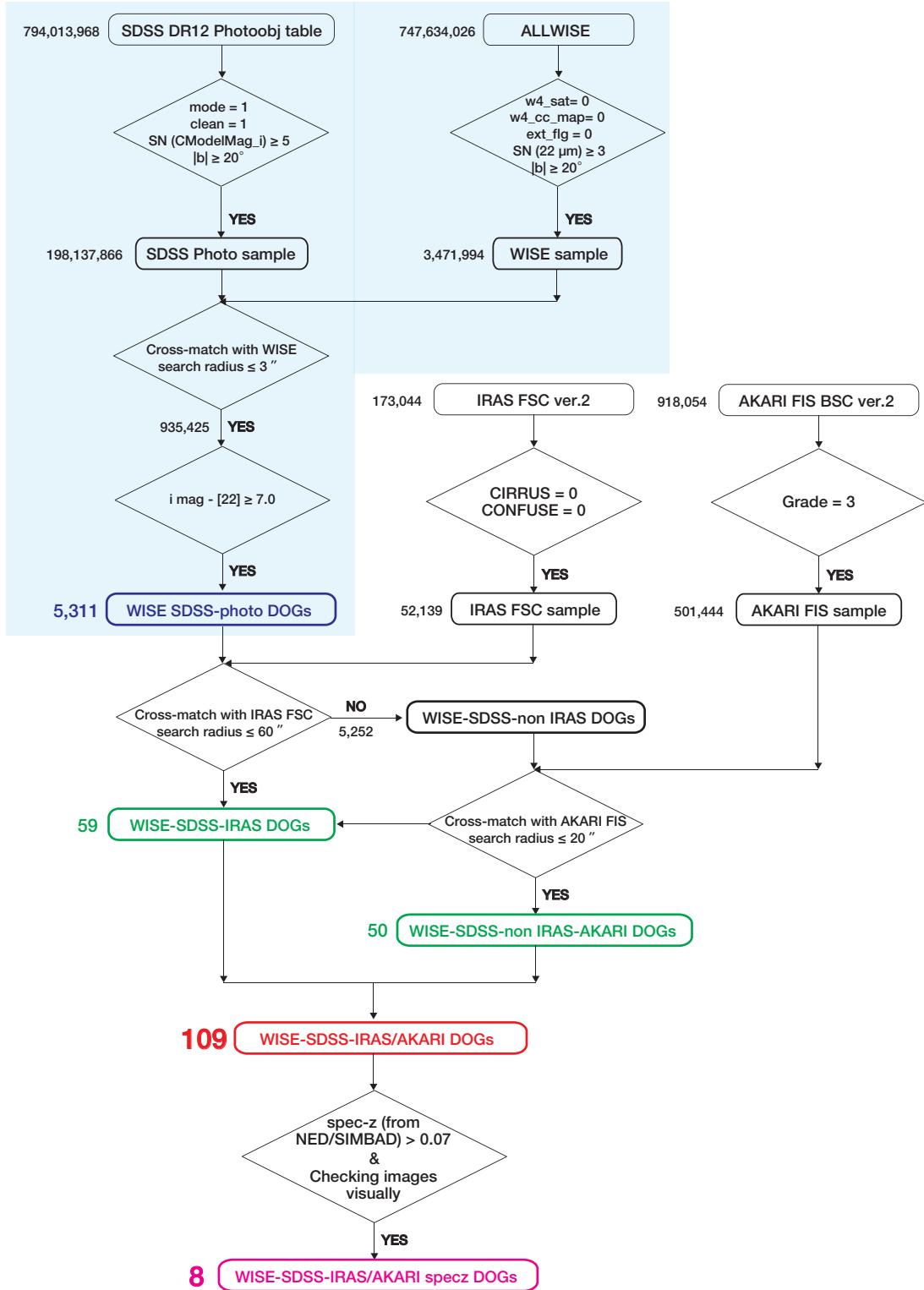


Figure 1. Flow chart of our DOGs selection process. Numbers in this figure denote the number of selected objects at each step. The blue-shaded part is exactly the same as Figure 1 of [Toba & Nagao \(2016\)](#).

selected $59 + 50 = 109$ DOGs (hereafter WISE–SDSS–IRAS/AKARI DOGs) in this work. The main difference of the WISE–SDSS–IRAS/AKARI DOGs and classical DOGs discovered by [Dey et al. \(2008\)](#) is the MIR flux; the typical (median) flux density at $22\ \mu\text{m}$ of our DOG sample is $10.4\ \text{mJy}$ that is much brighter than $0.3\ \text{mJy}$ at $24\ \mu\text{m}$ selected by [Dey et al. \(2008\)](#) (see also Section 4.2.2).

For the 109 WISE–SDSS–IRAS/AKARI DOGs, we compiled spectroscopic redshift information by utilizing the NASA/IPAC Extragalactic Database (NED²) and the Set of Identifications, Measurements, and Bibliography for Astronomical Data (SIMBAD) database³. For spectroscopically confirmed DOGs, we rejected nearby galaxies with redshift smaller than 0.07 to ensure the reliable photometry at each band because the photometry we employed is not optimized for extended sources (see Section 2.2). Finally, we visually checked optical, MIR, and FIR images and excluded a suspicious object that is affected by nearby bright star and/or that cannot be deblended by the SDSS pipeline. As a result, we selected 8 objects with spectroscopic redshift (hereafter WISE–SDSS–IRAS/AKARI specz DOGs) with $0.07 < z < 1.0$ (its mean redshift is ~ 0.54). We note that only one object has a SDSS spectrum with meaningful quality because the mean i -band magnitude of our DOG sample is ~ 19.4 that is fainter than that of typical SDSS spectroscopic galaxies. Figure 2 shows cutout images at optical, MIR, and FIR wavelength. All the information of our DOGs sample is tabulated in Table 2.

2.2. SED Fitting to derive the IR luminosity

We performed the SED fitting for the 8 WISE–SDSS–IRAS/AKARI specz DOG sample to derive the total IR luminosity, L_{IR} ($8\text{--}1000\ \mu\text{m}$). We employed the fitting code SED Analysis using Bayesian Statistics (SEABASs⁴: [Rovilos et al. 2014](#)) that provides up to three-component fitting (AGN, SF, and stellar component) based on the maximum likelihood method. For the AGN templates, we utilized the library of [Silva et al. \(2004\)](#), which contains torus templates with varying extinction ranging from $N_{\text{H}} = 0$ to $N_{\text{H}} = 10^{25}\ \text{cm}^{-2}$. For the SF templates, we utilized the library of [Chary & Elbaz \(2001\)](#) and [Mullaney et al. \(2011\)](#). We also used the library of [Polletta et al. \(2007\)](#) representing optically selected AGNs and SF galaxies (see [Polletta et al. 2007](#) for more detail). For the stellar templates, SEABASs gives a library of 1500 synthetic

stellar templates from [Bruzual & Charlot \(2003\)](#) stellar population models with solar metallicity and a range of SF histories and ages assuming a [Chabrier \(2003\)](#) initial mass function (IMF), and each model are reddened using a [Calzetti et al. \(2000\)](#) dust extinction law. In order to derive the total IR luminosity and stellar mass with small uncertainties, we used data only with $\text{fqual}_{25/60/100} \geq 2$ and $\text{fqual}_{65/69/140/160} = 3$ for *IRAS* and *AKARI* data, respectively. Eventually, we performed the SED fitting for 10–13 photometric points among u, g, r, i, z, J, H, K_s -band and $3.4, 4.6, 12, 22, 25, 60, 65, 90, 100, 140,$ and $160\ \mu\text{m}$ with SDSS, the TwoMicron All Sky Survey (2MASS: [Skrutskie et al. 2006](#)) Point Source Catalog (PSC: [Cutri et al. 2003](#)), *WISE*, *IRAS* and *AKARI* data, and estimated the total IR luminosity and stellar mass.

We employed the profile-fit magnitude and Cmodel-Mag for each source in the *WISE* and SDSS catalogs, respectively, which traces total flux (hereinafter we used $u, g, r, i,$ and z as a shorthand alias for CmodelMag). For the remaining photometry in 2MASS, *IRAS*, and *AKARI*, we used the default magnitude or flux in each catalog. Note that profile-fit photometry in *WISE* and default magnitude in 2MASS PSC are optimized for point sources and may underestimate the true brightness of extended sources. However, since we selected point like sources by adopting flags and redshift cut (see Section 2.1) and visually confirmed it, the photometry we used is reliable.

We took into account the equilibrium between the energy absorbed from the stellar component and the energy emitted in the IR by the SF. The uncertainties of the derived L_{IR} contains not only statistical error but also systematic error. SEABASs can calculate L_{IR} for “every” trial fit and estimate the likelihood value (corresponding to the chi-square) for each case, and provides us the uncertainties as the 2σ confidence interval. Therefore the influence of the difference between the inputted SED templates on the derived L_{IR} is included in the uncertainty.

3. RESULTS

3.1. Result of SED fitting

Figure 3 shows the example of the SED fitting. The best-fit AGN template for our IR-bright DOGs sample tends to favor the “torus” template presented by [Silva et al. \(2004\)](#) or [Polletta et al. \(2007\)](#), which is consistent with the report by [Tsai et al. \(2015\)](#) based on the WISE-selected IR luminous sources. A remarkable aspect we found is that IR-bright DOGs have a flat SED in MIR region which provides us a clue of an empirical relation of their MIR and IR luminosities (see Section 4.1). It should be noted that one object with

² <http://ned.ipac.caltech.edu/>

³ <http://simbad.u-strasbg.fr/simbad/>

⁴ <http://xraygroup.astro.noa.gr/SEABASs/>

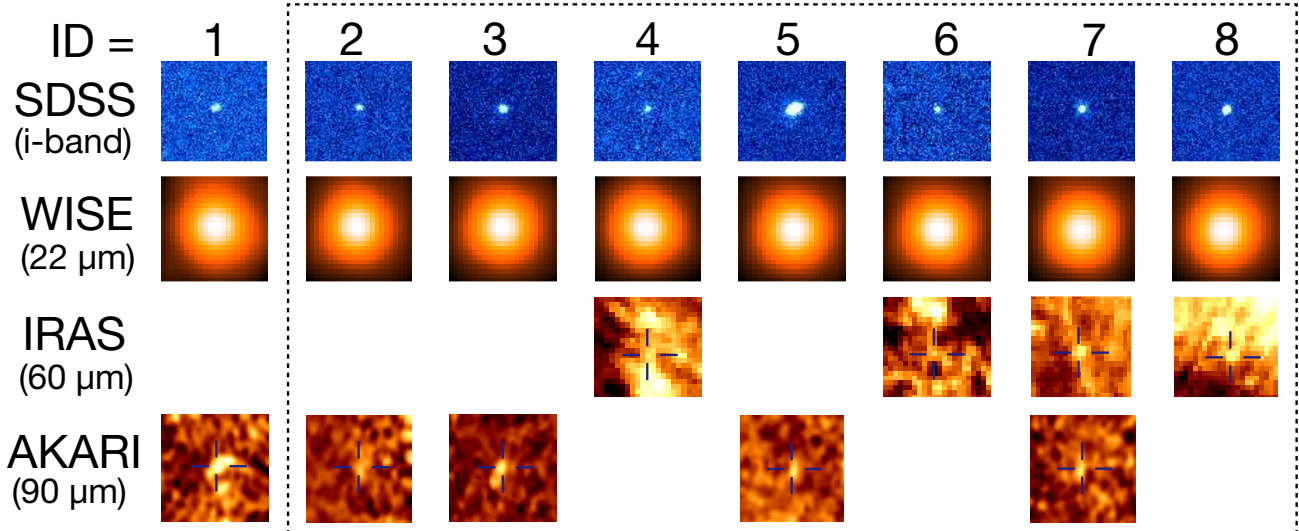


Figure 2. Cutout images at i -band (top), $22\ \mu\text{m}$ (upper-middle), $60\ \mu\text{m}$ (lower-middle), $100\ \mu\text{m}$ (bottom) taken by SDSS, WISE, IRAS, and AKARI, respectively. Each image is $30'' \times 30''$ for SDSS and WISE, $30' \times 30'$ for IRAS, and $10' \times 10'$ for AKARI in size, respectively. Note that we obtained the stellar mass and SFR for 7 objects with ID=2-8 (see Section 3.1).

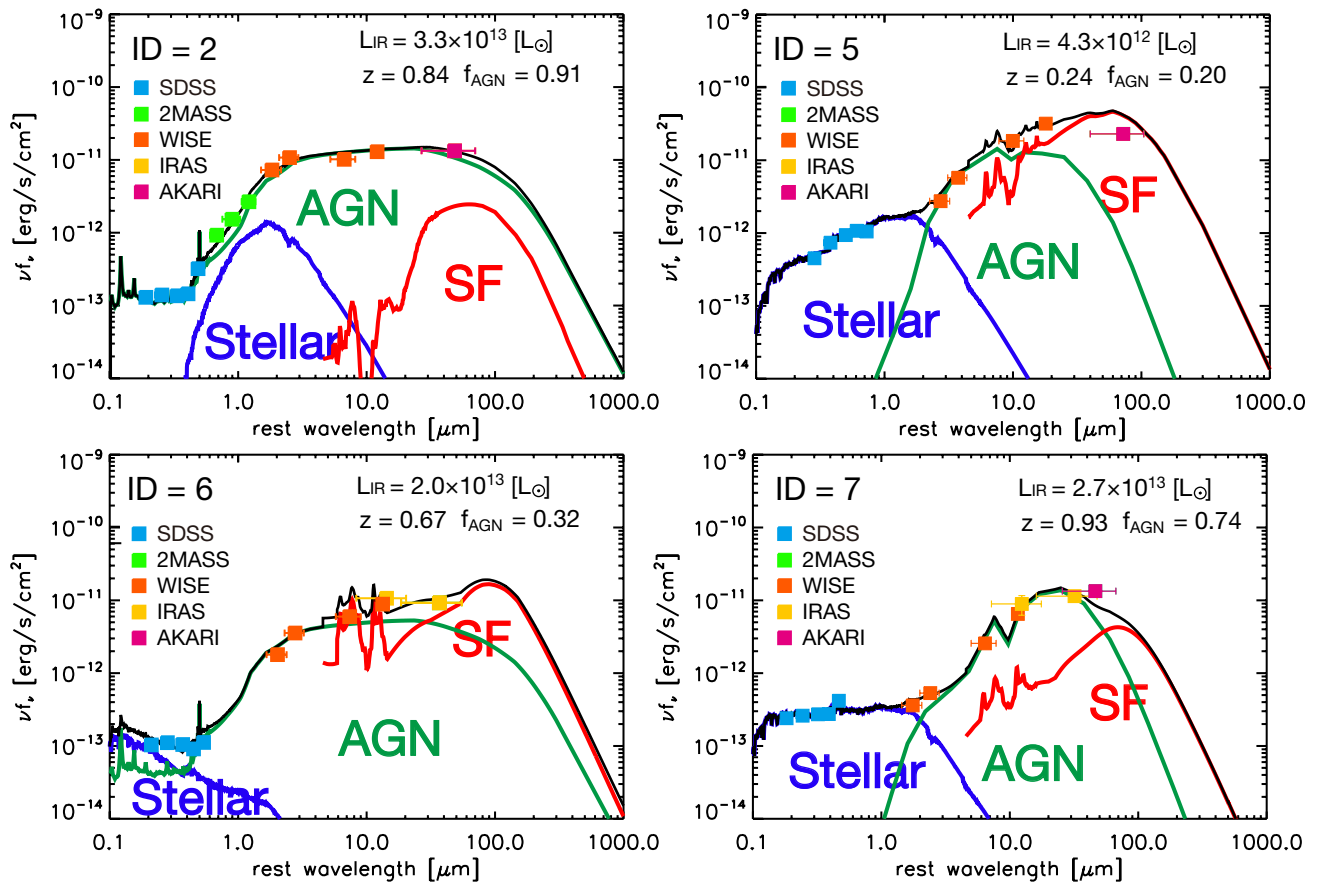


Figure 3. Examples of the SED fitting for our DOG sample. The blue, green, orange, yellow, and pink square represent the data from the SDSS, 2MASS, WISE, IRAS, and AKARI, respectively. The contribution from the stellar, AGN, SF components to the total SEDs are shown in blue, green, and red lines, respectively. The black solid line represents the resultant (the combination of the stellar, AGN, and SF) SEDs. We only used data with $f_{\text{qual}}_{25/60/100} \geq 2$ and $f_{\text{qual}}_{65/69/140/160} = 3$ for IRAS and AKARI data, respectively, for the SED fitting.

Table 2. The 8 WISE–SDSS–IRAS/AKARI specz DOGs identified in this work.

ID	FIS ID	objname	R.A. ^a	Decl. ^a	redshift ^b	<i>u</i> mag	<i>g</i> mag	<i>r</i> mag	<i>i</i> mag	<i>z</i> mag
			hms	dms		AB mag	AB mag	AB mag	AB mag	AB mag
1	5007582	AKARI J00260+1041	00:26:06.6	+10:41:26.5	0.57	21.89 ± 0.27	21.37 ± 0.06	20.37 ± 0.04	19.92 ± 0.05	19.79 ± 0.13
2	5204882	AKARI J09150+2418	09:15:01.7	+24:18:12.1	0.84	20.91 ± 0.06	20.59 ± 0.03	20.28 ± 0.03	19.95 ± 0.03	19.01 ± 0.04
3	5291698	AKARI J13070+2338	13:07:00.6	+23:38:05.1	0.28	21.46 ± 0.18	20.58 ± 0.03	19.38 ± 0.02	19.02 ± 0.02	18.56 ± 0.05
4	—	IRAS F13073+6057	13:09:16.9	+60:42:08.9	0.64	22.65 ± 0.32	22.91 ± 0.15	21.59 ± 0.12	20.47 ± 0.06	19.42 ± 0.11
5	5317429	AKARI J14063+0103	14:06:38.2	+01:02:54.5	0.24	19.40 ± 0.05	18.69 ± 0.01	18.10 ± 0.01	17.70 ± 0.01	17.64 ± 0.03
6	—	IRAS F14481+4454	14:49:53.6	+44:41:50.3	0.67	21.16 ± 0.08	20.74 ± 0.03	20.56 ± 0.03	20.47 ± 0.04	20.02 ± 0.14
7	5365228	AKARI J15324+3242	15:32:44.0	+32:42:46.6	0.93	20.18 ± 0.05	19.91 ± 0.02	19.53 ± 0.02	19.23 ± 0.02	18.40 ± 0.04
8	—	IRAS F23497-0448	23:52:15.1	-04:32:10.5	0.16	19.98 ± 0.07	19.47 ± 0.01	18.86 ± 0.01	18.74 ± 0.02	19.19 ± 0.09

<i>j</i> mag	<i>h</i> mag	<i>k</i> smag	3.4 μm flux	4.6 μm flux	12 μm flux	22 μm flux	25 μm flux (fqual_25)	60 μm flux (fqual_60)
AB mag	AB mag	AB mag	mJy	mJy	mJy	mJy	mJy	mJy
—	—	—	0.15 ± 0.01	0.13 ± 0.01	7.09 ± 0.29	29.68 ± 1.57	—	—
17.43 ± 0.17	16.59 ± 0.12	15.65 ± 0.04	8.20 ± 0.17	16.61 ± 0.31	41.92 ± 0.63	96.12 ± 2.41	—	—
17.66 ± 0.16	16.44 ± 0.07	15.31 ± 0.04	8.65 ± 0.18	14.71 ± 0.28	26.38 ± 0.42	75.79 ± 2.14	—	—
18.76	17.50 ± 0.24	16.64 ± 0.11	2.23 ± 0.05	4.23 ± 0.08	10.86 ± 0.22	26.94 ± 1.07	84.43 ± 17.73 (1)	194.70 ± 42.83 (3)
17.91 ± 0.20	17.51 ± 0.21	16.65 ± 0.13	3.09 ± 0.07	8.87 ± 0.18	75.79 ± 1.07	236.16 ± 4.45	—	—
—	—	—	2.02 ± 0.04	5.50 ± 0.10	24.57 ± 0.41	65.77 ± 1.65	85.09 ± 17.87 (2)	189.70 ± 32.25 (3)
—	—	—	0.41 ± 0.01	0.82 ± 0.02	10.55 ± 0.23	48.31 ± 1.22	71.03 ± 21.31 (2)	234.10 ± 35.12 (3)
—	—	—	0.19 ± 0.01	1.25 ± 0.03	18.78 ± 0.39	128.23 ± 2.98	311.50 ± 93.45 (1)	396.30 ± 67.37 (3)

65 μm flux (fqual_65)	90 μm flux (fqual_90)	100 μm flux (fqual_100)	140 μm flux (fqual_140)	160 μm flux (fqual_160)	log <i>L</i> _{IR}	log <i>M</i> _*	log SFR
mJy	mJy	mJy	mJy	mJy	<i>L</i> _☉	<i>M</i> _☉	<i>M</i> _☉ /yr
359.96 ± 250.89 (1)	417.40 ± 50.29 (3)	—	407.51 ± 231.02 (1)	—	—	—	—
—	396.88 ± 64.55 (3)	—	40.05 ± 258.74 (1)	—	13.52 ^{+0.04} _{-0.01}	12.60 ^{+0.18} _{-0.18}	2.56 ^{+0.25} _{-0.19}
453.78 ± 255.58 (1)	557.62 ± 61.57 (3)	—	507.33 ± 244.22 (1)	53.72 ± 338.50 (1)	12.33 ^{+0.06} _{-0.02}	9.86 ^{+0.10} _{-0.13}	1.95 ^{+0.12} _{-0.04}
—	—	818.30 ± 171.84 (1)	—	—	12.75 ^{+0.07} _{-0.11}	11.67 ^{+0.27} _{-0.11}	2.35 ^{+0.16} _{-0.53}
598.65 ± 252.74 (1)	684.26 ± 55.28 (3)	—	1332.88 ± 255.74 (1)	—	12.63 ^{+0.06} _{-0.07}	10.28 ^{+0.01} _{-0.17}	2.59 ^{+0.06} _{-0.10}
—	—	500.50 ± 115.12 (1)	—	—	13.29 ^{+0.12} _{-0.03}	9.16 ^{+0.08} _{-0.17}	3.16 ^{+0.15} _{-0.05}
61.96 ± 191.01 (1)	398.36 ± 46.21 (3)	711.80 ± 170.83 (1)	983.85 ± 189.00 (1)	433.56 ± 325.80 (1)	13.43 ^{+0.04} _{-0.01}	10.85 ^{+0.02} _{-0.00}	2.88 ^{+0.13} _{-0.04}
—	—	571.50 ± 165.73 (1)	—	—	11.98 ^{+0.09} _{-0.07}	9.65 ^{+0.01} _{-0.01}	1.94 ^{+0.09} _{-0.07}

^aThe coordinates in the SDSS DR12.^bNED.

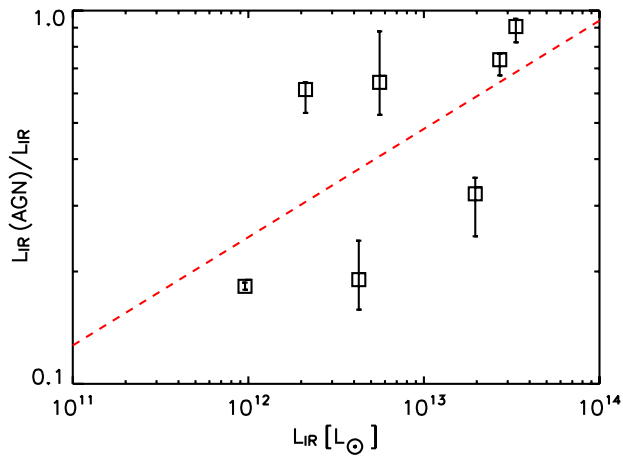


Figure 4. The luminosity contribution of AGN to the IR luminosity, $L_{\text{IR}}(\text{AGN})/L_{\text{IR}}$, as a function of IR luminosity. The red dotted line shows the best-fit linear function.

ID=1 cannot be well-fitted by SEABASs code. Its best-fit SED in FIR region provided significantly lower than observed flux at $90\ \mu\text{m}$. One possible reason is that this object has only one photometric point in the FIR regime that could not be enough to constrain the FIR SEDs. Another possibility is that its $90\ \mu\text{m}$ flux density might be overestimated due to the deblending issue and thus SEABASs with considering energy balance between UV/optical and IR cannot reproduce the FIR emission. Therefore, we excluded this object for the SED fitting and we derive the stellar mass, total IR luminosity, and SFR for the remaining 7 DOGs with ID=2-8 (see Table 2). Hereinafter, we focus on these objects.

3.2. Energy contribution of AGN to the IR luminosity

Since SEABASs executes the three-component SED fitting of stellar, AGN, and SF, we can calculate the energy contribution of each component to the IR luminosity. Figure 4 shows the luminosity contribution of AGN to the IR luminosity ($L_{\text{IR}}(\text{AGN})/L_{\text{IR}}$) as a function of IR luminosity. We found that the energy contribution of AGN to the IR luminosity increases with increasing the IR luminosity. This result is in good agreement with those from AKARI selected LIRGs/ULIRGs (e.g., Lee et al. 2012; Ichikawa et al. 2014) and those from IR-faint DOGs (e.g., Riguccini et al. 2015), in the sense that more IR-luminous sources tend to be more AGN-dominated. The fact that the luminous IR sources tend to be more AGN dominated relatively reported by several authors can be applicable for IR-bright DOGs.

4. DISCUSSIONS

4.1. Predicting L_{IR} from 22 and $90\ \mu\text{m}$ flux density

Here we discuss the correlation among the MIR luminosity, FIR luminosity, and total IR luminosity for IR-bright DOGs. As shown in Figure 3, the SEDs of

DOGs in MIR regime appears flat, which gives the possibility to estimate their IR luminosities from a MIR luminosity at “observed-frame” without considering k -correction. We derive 22 and $90\ \mu\text{m}$ luminosity density at observed frame, L_{ν}^{obs} ($22\ \mu\text{m}$ or $90\ \mu\text{m}$), just from the observed flux density by multiplying $4\pi d_L^2$ for each DOG, where d_L is luminosity distance.

Figure 5(a) shows the relation between the 22 and $90\ \mu\text{m}$ luminosity in the observed frame and IR luminosity. We see tight correlations between $22\ \mu\text{m}$ luminosity and IR luminosity, and $90\ \mu\text{m}$ luminosity and IR luminosity. Figure 5(b) shows the ratio of the 22 and $90\ \mu\text{m}$, and IR luminosity as a function of IR luminosity. The ratio of WISE $22\ \mu\text{m}$ and IR luminosity have similar value regardless of IR luminosity, which suggests that $22\ \mu\text{m}$ luminosity is a more linear relationship with IR luminosity. We obtained the following conversion formulae:

$$\log L_{\text{IR}} = (1.00 \pm 0.02) \log [\nu L_{\nu}^{\text{obs}}(22\ \mu\text{m})] + (0.48 \pm 0.28), \quad (1)$$

$$\log L_{\text{IR}} = (0.97 \pm 0.06) \log [\nu L_{\nu}^{\text{obs}}(90\ \mu\text{m})] + (0.76 \pm 0.79). \quad (2)$$

The Spearman rank correlation coefficients for each relationship are ~ 1.00 and 0.60 with null hypothesis probability $P \sim 0$ and 4.0×10^{-1} , respectively, indicating that $22\ \mu\text{m}$ luminosity can be used to predict the total IR luminosity for IR-bright DOGs with $0.07 < z < 1.0$ without considering k -correction. At the same time, we should keep in mind that whether or not this empirical relation is applicable to other galaxies is unknown, and thus this relation may be useful only for IR-bright DOGs.

4.2. Stellar mass and SFR

Since SEABASs has the advantage of being able to decompose the total SED into stellar, AGN, and SF components, we used IR luminosity contributed from SF activity and convert it to SFR using Kennicutt (1998) equation with the Chabrier IMF calibrated by Salim et al. (2016),

$$\text{SFR} = \log L_{\text{IR}}(\text{SF}) - 9.966. \quad (3)$$

where SFR and $L_{\text{IR}}(\text{SF})$ are given in unit of $M_{\odot}\ \text{yr}^{-1}$ and L_{\odot} , respectively. For the stellar mass, we used the output from the SED fitting based on SEABASs assuming same IMF. Note that the rest-frame UV continuum may be contributed by scattered light from AGNs particularly for luminous DOGs (e.g., Hamann et al. 2016), which induces an uncertainty for estimated stellar mass.

4.2.1. One to one comparison with literature

Before comparing SFR- M_{\star} relation of IR-bright DOG sample with those of other population, we investigate

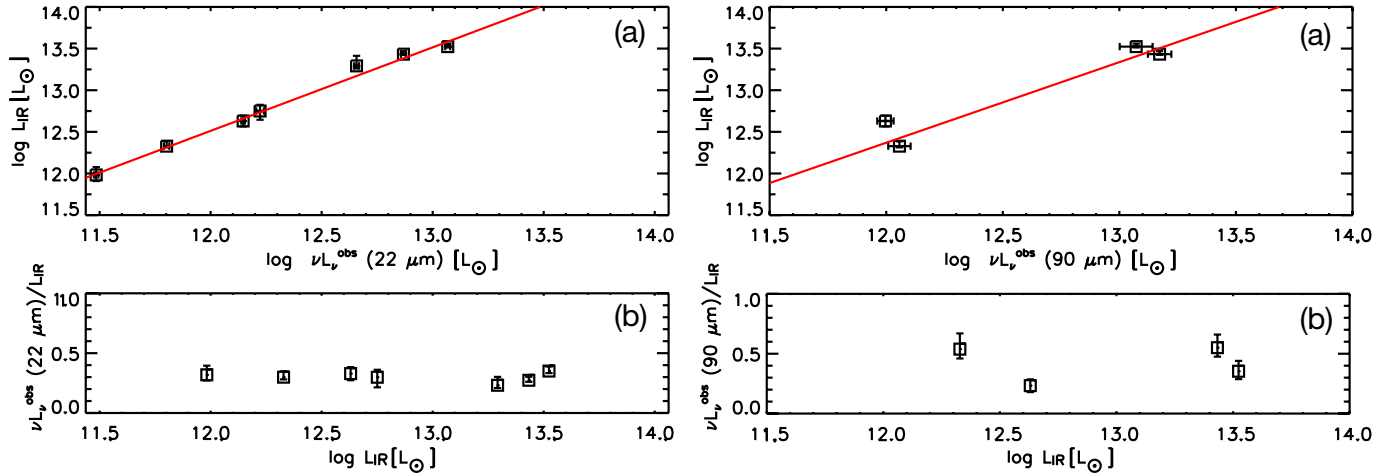


Figure 5. (a) *WISE* 22 μm luminosity at observed frame vs. IR luminosity (left) and *AKARI* 90 μm luminosity at observed frame vs. IR luminosities (right). The red dotted line shows the best-fit linear function. (b) The ratio of 22 μm (left) and 90 μm (right), and IR luminosity as a function of IR luminosity.

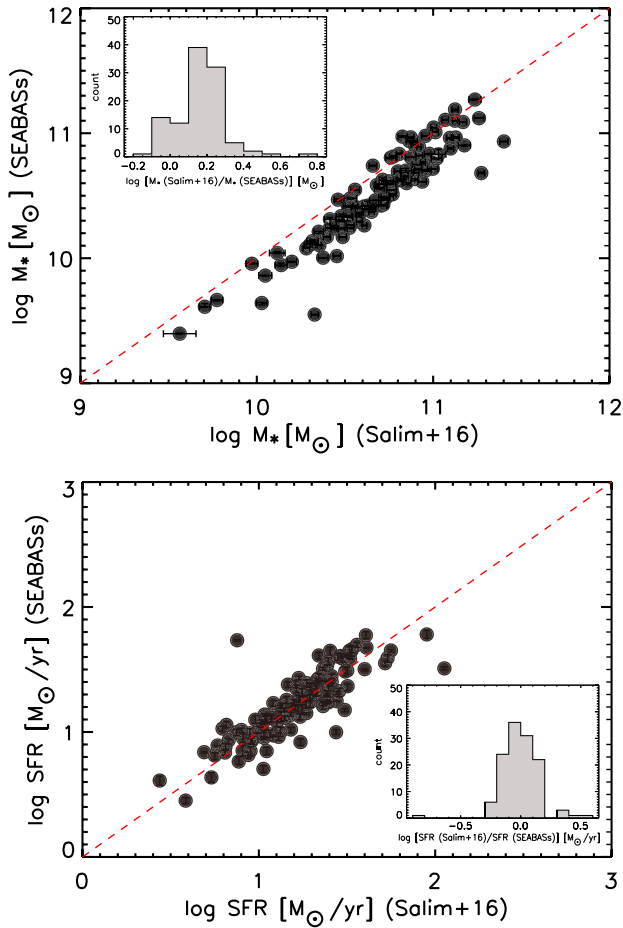


Figure 6. Comparison of stellar mass (top) and SFR (bottom) derived by *SEABAS* we employed in this work and [Salim et al. \(2016\)](#). The red dotted line is the one-to-one line. The inserted figure shows the histogram of the ratio of each quantity derived in this work and [Salim et al. \(2016\)](#) for stellar mass (top) and SFR (bottom), respectively.

whether or not the estimate of stellar mass and SFR based on *SEABAS* have a systematic offset compared to those derived from previous works using some local galaxies/ULIRGs. One caution here is that the difference of the assumed IMF also affects the stellar mass and SFR (e.g., [Rieke et al. 2009](#); [Casey et al. 2014](#)), which induces a systematic offset on SFR– M_* plane. Therefore, we corrected the stellar mass and SFR in the literature to those assumed Chabrier IMF by dividing them by 1.58 [Salim et al. \(2007\)](#) (see also [Tacconi et al. 2008](#)) if needed.

First, we compare stellar mass and SFR with those of local galaxies at $z < 0.3$ estimated by [Salim et al. \(2007\)](#). They recently provided a catalog (GALEX–SDSS–WISE Legacy Catalog: GSWLC) of physical properties including stellar masses and SFRs that were derived by the SED fitting following a Bayesian methodology for UV/optical data. Note that in addition to SFRs derived from the SED fitting, they provided MIR SFRs derived from IR templates based on *WISE* 22 μm data to avoid potential systematics. This is because they do not use the FIR data to derive the SFR that could induce large uncertainties (see e.g., [Toba & Nagao 2016](#)). So, we first cross matched the GSWLC catalog with *AKARI* FIS BSC ver.2, and derived stellar mass and SFR of matched sources as described above. We then compared each quantity of them with those in GSWLC where we used MIR-SFR derived from ALLWISE catalog.

Figure 6 shows the comparison of stellar masses derived from our method and those in GSWLC. Our estimate of SFR is in good agreement with that in [Salim et al. \(2007\)](#) while the stellar mass we estimated is slightly smaller than that in [Salim et al. \(2007\)](#); the typical offset of stellar mass is ~ 0.15 dex. This offset is roughly consistent with that results from the comparison

between GSWLC and the Max Planck Institute for Astrophysics/Johns Hopkins University (MPA/JHU) catalog (Kauffmann et al. 2003; Brinchmann et al. 2004) (see Salim et al. 2007, in detail). We should keep in mind this offset when comparing the stellar masses with local SDSS galaxies.

Next, we compare stellar mass and SFR with those of local ULIRGs at $z < 0.3$ estimated by Kilerci, Goto, & Doi (2014). They constructed a ULIRG sample by cross-matching the *AKARI* FIS BSC version 1 (Yamamura et al. 2010) with the SDSS DR10 (Ahn et al. 2014). Figure 7 shows the comparison of stellar masses and SFRs derived from our method and those in Kilerci, Goto, & Doi (2014). Our estimate of SFR is roughly consistent with that in Kilerci, Goto, & Doi (2014) although we underestimate significantly SFR for some ULIRGs, while the stellar mass we estimated is obviously larger than that in Kilerci, Goto, & Doi (2014); the typical offset of stellar mass is ~ 0.5 dex. We note that Kilerci, Goto, & Doi (2014) reported that all of the adopted stellar mass values in their work might be underestimated by ~ 0.5 dex by comparing the derived stellar mass with previous works, which could be a possible interpretation of the discrepancy of our estimate of stellar mass. We should keep in mind this offset when comparing the stellar mass with local ULIRGs.

4.2.2. Stellar mass and SFR relation

We discuss where IR-bright DOGs lie in SFR– M_* plane and compare it with that of the literature. We first estimated the SFR based on the IR luminosity from SF.

Figure 8 shows the resultant stellar mass and SFR relation for our DOG sample, the main-sequence (MS) sample for star forming galaxies selected by the SDSS and *WISE* (Chang et al. 2015), and selected by the Galaxy Evolution Explorer (*GALEX*) satellite (Martin et al. 2005), SDSS, and *WISE* (Salim et al. 2016). The stellar mass and SFR of the MS presented by Elbaz et al. (2007) and Daddi et al. (2007) for star forming galaxies at $z = 1$ and 2, respectively, are also shown in Figure 8. Note that we corrected a possible offset of stellar masses discussed in Section 4.2.1 for local SDSS sample provided by (Salim et al. 2016). We remind that we corrected the stellar mass and SFR in the literature to those assumed Chabrier IMF if needed. We found that most IR-bright DOGs lie above these relations significantly although the redshift of our DOG sample is less than 1.0. They cover a locus of merger-driven starburst galaxies (e.g., Rodighiero et al. 2011), indicating that our IR-bright DOG sample detected by *IRAS* and/or *AKARI* is basically starburst galaxies. The stellar mass and SFR of a ULIRG sample presented

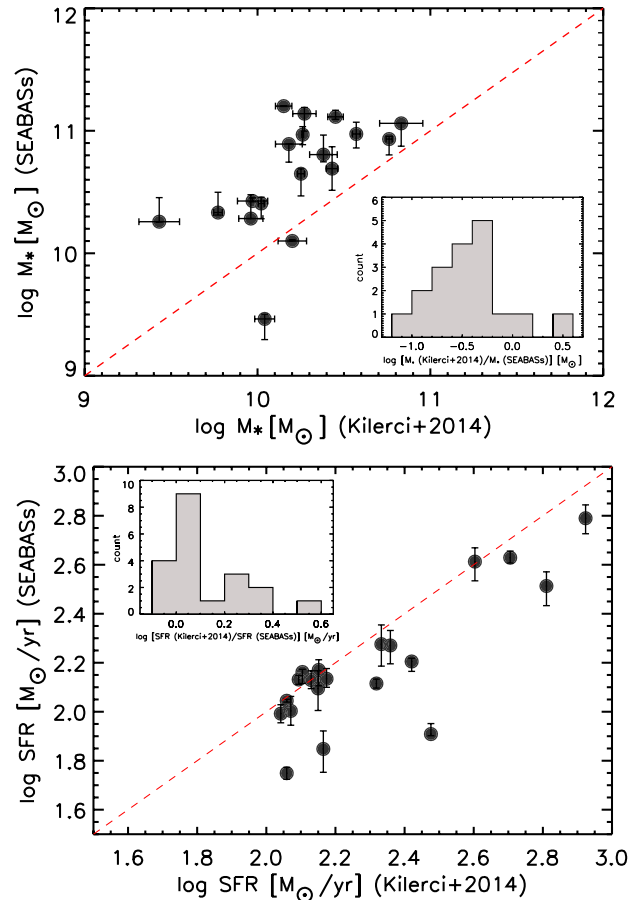


Figure 7. Comparison of stellar mass (top) and SFR (bottom) derived by SEABASS we employed in this work and Kilerci, Goto, & Doi (2014). The red dotted line is the one-to-one line. The inserted figure shows the histogram of the ratio of each quantity derived in this work and Kilerci, Goto, & Doi (2014) for stellar mass (top) and SFR (bottom), respectively.

by Kilerci, Goto, & Doi (2014) are also plotted. We also corrected a possible offset of stellar masses discussed in Section 4.2.1 for them. We found that some IR-bright DOGs have larger SFR value given a same stellar mass (although remaining objects overlapped with local ULIRGs in SFR– M_* plane.) This is partially due to the difference of the redshift distribution; redshift of sample in Kilerci, Goto, & Doi (2014) is less than 0.5. However, it is difficult to conclude this offset is statistically robust due to small sample size, and thus it will be future work. The tendency of the large offset of IR-bright DOG from MS in SFR– M_* plane is likely to be inconsistent with that of IR-faint DOGs (Kartaltepe et al. 2012; Riguccini et al. 2015). They reported that IR-faint DOGs with no significant AGN contribution are mainly located within the star-forming MS, although some author reported that they are widely distributed on SFR– M_* plane (Calanog et al. 2013; Corral et al. 2016). Note that our sample is relatively low-redshift ($z \sim 0.54$) compared with IR-faint DOG sample ($z \sim 2$).

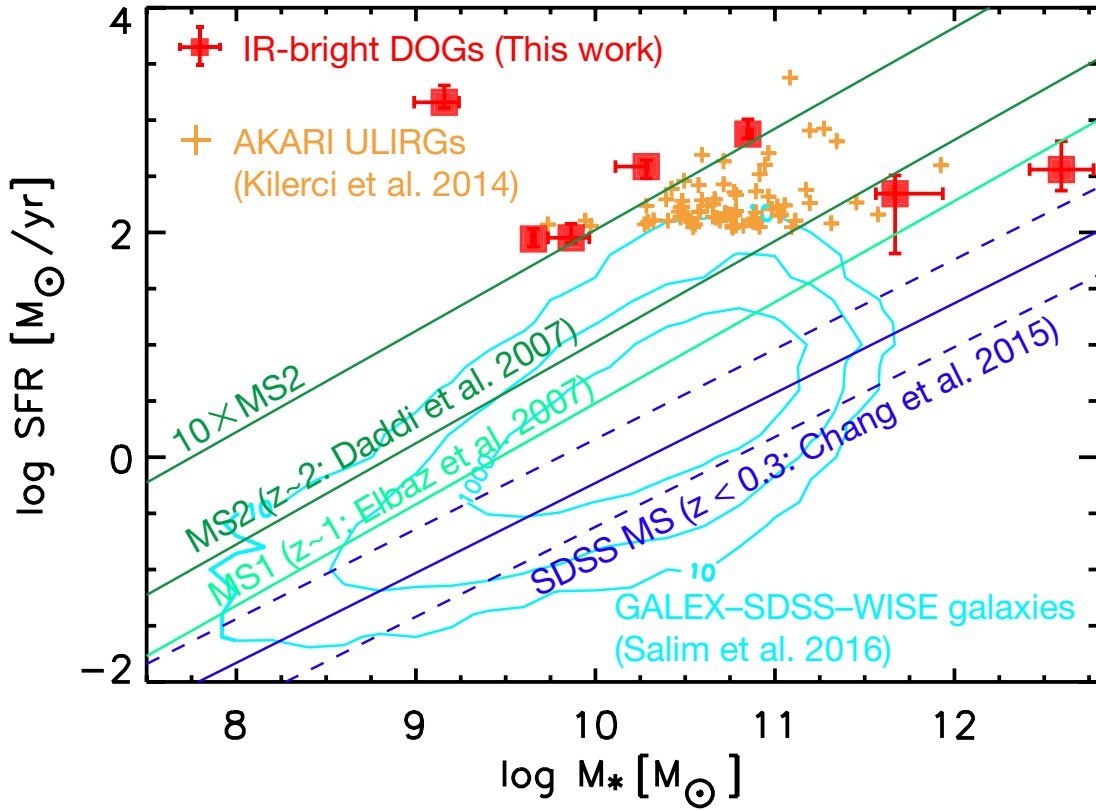


Figure 8. Stellar mass and SFR for 7 IR-bright DOGs (red square) and 75 AKARI-selected ULIRGs (Kilerci, Goto, & Doi 2014). The blue solid line is main sequence (MS) of normal SF galaxies selected from the SDSS (Chang et al. 2015) with scatter of 0.39 dex (blue dotted line). The cyan contours represent SFR- M_* relation for a sample of GALEX-SDSS-WISE Legacy Catalog (GSWLC: Salim et al. 2016) at $z < 0.3$. The bin size is 0.2×0.2 in the units given in the plot. The light green line is MS of normal SF galaxies at $z = 1$ (Elbaz et al. 2007) while the dark green lines are MS of SF galaxies at $z = 2$ (Daddi et al. 2007) and 10 times above this relationship.

Also, the MIR flux range of them is significantly different. Taking these results into account, the SF properties of IR-bright DOGs is not necessary to same as IR-faint (i.e., classical) DOGs. This work enables us to constrain SFR- M_* relation of previously unknown, IR-bright DOGs whose properties differ from those of classical, IR-faint DOGs, for the first time.

It should be noted that SFR- M_* relation of MS is also related to its other physical properties such as metallicity (e.g., Mannucci et al. 2010), molecular gas fraction (e.g., Daddi et al. 2010; Sargent et al. 2014), and starburst compactness (e.g., Elbaz et al. 2011). However, a full exploitation of how each physical property of IR-bright DOGs affects the SFR- M_* relation requires a further observation to derive each quantity, which is beyond the scope of this paper, and will be a future work. We here just discuss a possibility of that the large offset of our DOG sample from MS can be explained depending on the metallicity of IR-bright DOGs and MS. Since the dispersion of SFR and stellar mass due to the metallicity of MS is 0.2-0.4 dex (Savaglio et al. 2005; Lara-López et al. 2012), the large offset of IR-bright DOGs cannot be explained only by metallic-

ity. Therefore, taking the redshift evolution of SFR- M_* relation (Whitaker et al. 2012; Lee et al. 2015; Tomczak et al. 2016) and uncertainty of SFR- M_* for MS due to the dispersion of at least metallicity into account, our IR-bright DOGs detected by *IRAS* and/or *AKARI* seems to be more specific population compared with IR-faint DOGs regarding the SFR- M_* relation.

The authors appreciate the referee’s thoughtful feedback which improved the manuscript. This research is based on observations with *AKARI*, a JAXA project with the participation of ESA. This research has made use of the NASA/ IPAC Infrared Science Archive, which is operated by the Jet Propulsion Laboratory, California Institute of Technology, under contract with the National Aeronautics and Space Administration. This publication makes use of data products from the Wide-field Infrared Survey Explorer, which is a joint project of the University of California, Los Angeles, and the Jet Propulsion Laboratory/California Institute of Technology, funded by the National Aeronautics and Space Administration. Funding for SDSS-III has been provided by the Alfred P. Sloan Foundation, the Partic-

icipating Institutions, the National Science Foundation, and the U.S. Department of Energy Office of Science. The SDSS-III web site is <http://www.sdss3.org/>. SDSS-III is managed by the Astrophysical Research Consortium for the Participating Institutions of the SDSS-III Collaboration including the University of Arizona, the Brazilian Participation Group, Brookhaven National Laboratory, Carnegie Mellon University, University of Florida, the French Participation Group, the German Participation Group, Harvard University, the Instituto de Astrofísica de Canarias, the Michigan State/Notre Dame/JINA Participation Group, Johns Hopkins University, Lawrence Berkeley National Laboratory, Max Planck Institute for Astrophysics, Max Planck Institute for Extraterrestrial Physics, New Mexico State University, New York University, Ohio State University, Pennsylvania State University, University of Portsmouth, Princeton University, the Spanish Participation Group, University of Tokyo, University of Utah, Vanderbilt University, University of Virginia, University of Washington, and Yale University. This publication makes

use of data products from the Two Micron All Sky Survey, which is a joint project of the University of Massachusetts and the Infrared Processing and Analysis Center/California Institute of Technology, funded by the National Aeronautics and Space Administration and the National Science Foundation. This publication makes use of data products from the Two Micron All Sky Survey, which is a joint project of the University of Massachusetts and the Infrared Processing and Analysis Center/California Institute of Technology, funded by the National Aeronautics and Space Administration and the National Science Foundation. This research has made use of the NASA/IPAC Infrared Science Archive, which is operated by the Jet Propulsion Laboratory, California Institute of Technology, under contract with the National Aeronautics and Space Administration. Y.Toba and W.-H.Wang acknowledge the support from the Ministry of Science and Technology of Taiwan (MOST 102-2119-M-001-007-MY3 and 105-2112-M-001-029-MY3). TN is financially supported by the Japan Society for the Promotion of Science (JSPS) KAKENHI (16H01101 and 16H03958).

REFERENCES

- Ahn, C. P., Alexandroff, R., Allende Prieto, C., et al. 2014, *ApJS*, 211
- Alam, S., Albareti, F. D., Allende Prieto, C., et al. 2015, *ApJS*, 219, 12
- Beichman, C. A., Neugebauer, G., Habing, H. J., Clegg, P. E., & Chester, T. J. (ed.) 1988, in *Infrared Astronomical Satellite (IRAS) Catalogs and Atlases Volume 1: Explanatory Supplement* (Washington, DC: NASA)
- Brinchmann, J., Charlot, S., White, S. D. M., et al. 2004, *MNRAS*, 351, 1151
- Bruzual, G., & Charlot, S. 2003, *MNRAS*, 344, 1000
- Bussmann, R. S., Dey, A., Armus, L., et al. 2012, *ApJ*, 744, 150
- Calanog, J. A., Wardlow, J., Fu, H., et al. 2013, *ApJ*, 775, 61
- Calzetti, D., Armus, L., Bohlin, R. C., et al. 2000, *ApJ*, 533, 682
- Casey, C. M., Narayanan, D., & Cooray, A. 2014, *Physics Reports*, 541, 45
- Chabrier, G. 2003, *PASP*, 115, 763
- Chang, Y.-Y., van der Wel, A., da Cunha, E., & Rix, H.-W. 2015, *ApJS*, 219
- Chary, R., & Elbaz, D. 2001, *ApJ*, 556, 562
- Corral, A., et al. 2016, *A&A*, 592, 109
- Cutri, R. M., & et al. 2014, *VizieR Online Data Catalog*, 2328, 0
- Cutri, R. M., Skrutskie, M. F., van Dyk, S., et al. 2003, *2MASS All Sky Catalog of point sources*
- Daddi, E., Dickinson, M., Morrison, G., et al. 2007, *ApJ*, 670, 156
- Daddi, E., et al. 2010, *ApJL*, 714, L118
- Dey, A., Soifer, B. T., Desai, V., et al. 2008, *ApJ*, 677, 943
- Elbaz, D., Daddi, E., Le Borgne, D., et al. 2007, *A&A*, 468, 33
- Elbaz, D., et al. 2011, *A&A* 533, 119
- Hamann, F., Zakamska, N. L., Ross, N., et al. 2017, *MNRAS*, 464, 3431
- Hopkins, P. F., Hernquist, L., Cox, T. J., & Kereš, D. 2008, *ApJS*, 175, 356
- Ichikawa, K., Imanishi, M., Ueda, Y., et al. 2014, *ApJ*, 794, 139
- Kartaltepe, J. S., et al. 2012, *ApJ*, 757, 23
- Kauffmann, G., et al. 2003, *MNRAS*, 341, 54
- Kawada, M., Baba, H., Barthel, P. D., et al. 2007, *PASJ*, 59, 389
- Kennicutt, R. C., Jr. 1998, *ARA&A*, 36, 189
- Kilerci Eser, E., Goto, T., & Doi, Y. 2014, *ApJ*, 797
- Koyama, Y., Smail, I., Kurk, J., et al. 2013, *MNRAS*, 434, 423
- Lara-López, M. A., Bongiovanni, A., Cepa, J., et al. 2010, *A&A*, 519
- Lee, J. C., Hwang, H. S., Lee, M. G., Kim, M., & Lee, J. H. 2012, *ApJ*, 756, 95
- Lee, N., Sanders, D. B., Casey, C. M., et al. 2015, *ApJ*, 801
- Mannucci, F., Cresci, G., Maiolino, R., Marconi, A., & Gnerucci, A. 2010, *MNRAS*, 408, 2115
- Martin, D. C., Fanson, J., Schiminovich, D., et al. 2005, *ApJL*, 619, L1
- Moshir, M., Kopman, G., & Conrow, T. A. O. 1992, *IRAS Faint Source Survey, Explanatory Supplement Version 2* (Pasadena, CA: California Institute of Technology)
- Mullaney, J. R., Alexander, D. M., Goulding, A. D., & Hickox, R. C. 2011, *MNRAS*, 414, 1082
- Murakami, H., Baba, H., Barthel, P., et al. 2007, *PASJ*, 59, 369
- Neugebauer, G., Habing, H. J., van Duinen, R., et al. 1984, *ApJL*, 278, L1
- Noeske, K. G., Weiner, B. J., Faber, S. M., et al. 2007, *ApJL*, 660, L43
- Polletta, M., Tajer, M., Maraschi, L., et al. 2007, *ApJ*, 663, 81
- Rieke, G. H., Alonso-Herrero, A., Weiner, B. J., Pérez-González, P. G., Blaylock, M., Donley, J. L., & Marcillac, D. 2009, *ApJ*, 692, 556
- Riguccini, L., Le Floch, E., Mullaney, J. R., et al. 2015, *MNRAS*, 452, 470
- Rodighiero, G., Daddi, E., Baronchelli, I., et al. 2011, *ApJL*, 739
- Rovilos, E., Georgantopoulos, I., Akylas, A., et al. 2014, *MNRAS*, 438, 494
- Salim, S., Lee, J. C., Janowiecki, S., et al. 2016, *ApJS*, 227
- Salim, S., et al. 2007, *ApJS*, 173, 267
- Sanders, D. B., & Mirabel, I. F. 1996, *ARA&A*, 34, 749
- Sargent, M. T., et al. 2014, *ApJ*, 793, 19

- Savaglio, S., Glazebrook, K., Le Borgne, D., et al. 2005, *ApJ*, 635, 260
- Silva, L., Maiolino, R., & Granato, G. L. 2004, *MNRAS*, 355, 973
- Skrutskie, M. F., Cutri, R. M., Stiening, R., et al. 2006, *AJ*, 131, 1163
- Tacconi, L. J., et al. 2008, *ApJ*, 680, 246
- Taylor, M. B., Britton, M., & Ebert, R. 2005, in *Astronomical Data Analysis Software and Systems XIV*, ed. P. Shopbell, 29
- Toba, Y., Nagao, T., Kajisawa, M., et al. 2017, *ApJ*, 835, 36
- Toba, Y., & Nagao, T. 2016, *ApJ*, 820, 46
- Toba, Y., Nagao, T., Strauss, M. A., et al. 2015, *PASJ*, 67, 86
- Tomczak, A. R., Quadri, R. F., Tran, K.-V. H., et al. 2016, *ApJ*, 817
- Tsai, C.-W., Eisenhardt, P. R. M., Wu, J., et al. 2015, *ApJ*, 805, 90
- Whitaker, K. E., van Dokkum, P. G., Brammer, G., & Franx, M. 2012, *ApJL*, 754
- Wright, E. L., Eisenhardt, P. R. M., Mainzer, A. K., et al. 2010, *AJ*, 140, 1868
- Yamamura, I., Makiuti, S., Ikeda, N., et al. 2010, *yCat*, 2298, 0
- York, D. G., Adelman, J., Anderson, J. E., Jr., et al. 2000, *AJ*, 120, 1579